

Cu Diffusion-Driven Dynamic Modulation of the Electrical Properties of Amorphous Oxide Semiconductors

Han-Wool Yeon, Janghyun Jo, Hochul Song, Youngho Kang, Sekwon Na, Hyobin Yoo, Seung-Yong Lee, Haelim Cho, Ho-Young Kang, Jung-Kyu Jung, Seungwu Han, Miyoung Kim, and Young-Chang Joo*

The exact role of Cu in the electrical properties of amorphous oxide semiconductors (AOSs) has been unclear, even though Cu has been the key element for the p-type characteristics of crystalline oxide semiconductors. Here, the dynamic changes, determined by diffusion kinetics, in the effect of Cu on the electrical properties of amorphous In–Ga–Zn–O (a-IGZO) are revealed. In the early stage of annealing, Cu dominantly diffuses into a-IGZO through the free volume and acts as a mobile electron donor, which generates a resistive switching (RS) behavior related to the conductive filaments (CFs). With further annealing, substitutional Cu becomes predominant via In sites. After annealing, supersaturated Cu forms nonuniform, crystalline Cu–In–O clusters in a-IGZO, which decrease the electrical conductivity of a-IGZO and deteriorate the CF-based RS performance. The findings reveal Cu diffusion mechanisms and the role of Cu in the electrical properties of AOSs dependent on the structural location and provide guidelines for modulating the RS characteristics of AOSs through Cu diffusion control.

1. Introduction

Cu is the vital base element in crystalline metal-oxides to create p-type semiconductors.^[1–3] Cu suppresses the formation of oxygen vacancies (V_{O}) which are a n-type defect,^[3] and enhances hole mobility by reducing the localization of the valence band maximum, which is a hole conduction path.^[1,2] Furthermore, Cu has been used as a p-type dopant in crystalline oxide semiconductors to modulate electrical properties,^[4,5] even changing the conduction type from n-type to p-type when Cu concentration reaches the level of atomic percent (i.e., heavy doping).^[6] Interestingly, the exact role of Cu in amorphous oxide semiconductors remains unknown, although the

intriguing phenomenon that the amorphization of Cu-based crystalline oxides has induced a loss of p-type semiconducting characteristics, resulting in insulating properties, has been reported.^[7]

Amorphous (i.e., long-range disordered) structures are favorable for oxide semiconductors because they improve the film uniformity and mechanical flexibility.^[8,9] Moreover, n-type amorphous oxide semiconductors (AOSs) such as amorphous In–Ga–Zn–O (a-IGZO) have similar electrical properties to the corresponding crystalline oxides.^[8,9] Because of these advantages, n-type AOSs have been actively investigated for implementation in next-generation device platforms such as large-area, flexible, and transparent electronic devices (optical energy band gap of a-IGZO, ≈ 3.2 eV).^[8–11] An identification of the fundamental role of Cu in the electrical

properties of AOSs would be one of the most momentous steps for the continuous development of amorphous oxide electronics.

However, to date, investigations of the effect of Cu on the electrical properties of AOSs have been conducted solely in terms of the reliability of AOS electronics,^[12–16] similar to the investigation of conventional semiconductor (e.g., Si, Ge) devices^[17–19] (cf., Cu doping was used to form a passivation layer on an a-IGZO thin-film surface to prevent plasma-induced damages^[20]). Because Cu is frequently used as the interconnecting metal to reduce resistance–capacitance (R – C) delay at back-end of the line, Cu contamination has been a concern in terms of the deteriorating electrical performance of AOS devices.^[12–16] In previous reports, certain researchers suggested that a Cu impurity acts as an acceptor-like trap,^[14–16] whereas other researchers reported that Cu forms donor-like states in the subgap region.^[13] Thus, disagreement exists with regard to the electronic states of Cu in AOSs, although all previous studies were conducted using AOS thin-film transistors (TFTs) composed of Cu electrodes. If Cu diffusion into AOSs from the Cu electrodes is the dominant origin of the electrical degradation of AOS TFTs, the Cu diffusion length should be at least $3 \mu\text{m}$ (i.e., the minimum AOS channel length of TFTs in the reports) during annealing at below 300°C for 1 h.^[17–19] Based on the equation, $L = \sqrt{D_{\text{Cu}}t}$ (where L is the diffusion length, t is the diffusion time, and D_{Cu} is the Cu diffusivity

Dr. H.-W. Yeon, J. Jo, H. Song, Dr. Y. Kang, Dr. S. Na, Dr. H. Yoo, Dr. S.-Y. Lee, H. Cho, H.-Y. Kang, Dr. J.-K. Jung, Prof. S. Han, Prof. M. Kim, Prof. Y.-C. Joo
Department of Materials Science and Engineering
Seoul National University
Seoul 151-744, Republic of Korea
E-mail: ycjoo@snu.ac.kr

Prof. Y.-C. Joo
Research Institute of Advanced Materials (RIAM)
Seoul National University
Seoul 151-742, Republic of Korea

DOI: 10.1002/adfm.201700336

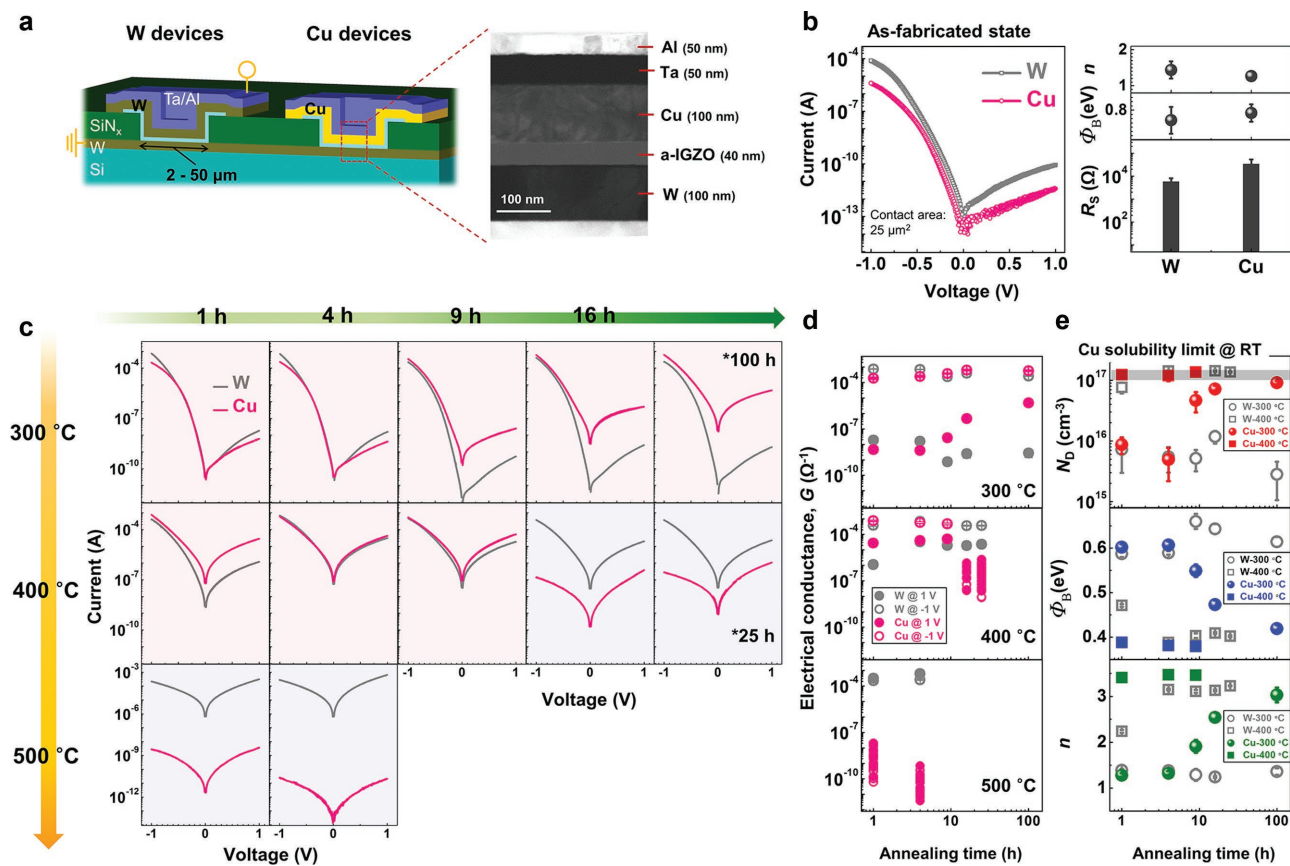


Figure 1. *I*–*V* characteristics. a) Schematic structure of the W devices and Cu devices composed of 40 nm thick a-IGZO thin-film patches. A cross-sectional TEM image of the Cu devices in the as-fabricated state is shown as well. b) The representative *I*–*V* characteristics in the as-fabricated devices (measured at RT). The contact area of the devices is 25 μm². c) *I*–*V* map and d) *G* (at ±1 V) of the 25 μm² devices considering both the annealing temperature from 300 to 500 °C and the annealing time from 1 to 100 h. e) The variations of Φ_B, *n*, and *N*_D in the Schottky conducting devices with respect to annealing conditions.

in AOSs),^[21] the extracted D_{Cu} values ($>10^{-10}$ cm² s⁻¹) are outrageously high compared to the Cu diffusivity determined in several amorphous oxides ($\approx 10^{-15}$ cm² s⁻¹).^[22–24] Therefore, Cu diffusion may be not the dominant origin of electrical degradation in AOS TFTs, and unpredicted factors could cause degradation during annealing. Although Jeong et al., suggested that Cu doping occurs by electrochemical migration,^[13] the nature of the Cu doping resulting from an electrochemical potential gradient^[19,25] is completely different from the Cu doping from a chemical potential gradient.^[22] Thus, the effects of diffusion-driven Cu doping on the electrical properties of AOSs have yet to be revealed. An in-depth understanding of the Cu diffusion mechanisms in AOSs is necessary to unravel the exact electronic state of Cu in AOSs.

Here, we reveal the effect of Cu on the electrical properties of AOSs through investigating the changes in the electrical properties of vertical-structure Cu/AOS/W devices with respect to various annealing temperatures and times. The cross-sections of the Cu/a-IGZO/W devices (Cu devices) are schematically depicted in Figure 1a. Cu diffusion occurs from Cu in the top electrode (TE), and the diffused Cu accumulates in the bulk a-IGZO because both the SiN_x isolation layer and W bottom electrode (BE) act as a Cu diffusion barrier.^[26,27] Changes in the current–voltage (*I*–*V*) characteristics of the Cu devices

with respect to the postfabrication annealing conditions were analyzed. Moreover, the changes in the electric field-induced electrical breakdown behavior of the Cu devices were investigated. We previously reported the increase in the free electron concentration in a-IGZO in W/a-IGZO/W devices (W devices) after annealing due to structural relaxation (SR)-driven doping. During annealing at below the glass transition temperature, the interactions between W and a-IGZO are negligible, and the free volume in a-IGZO is reduced (i.e., SR), resulting in an increase in the doping concentration (N_D).^[28] By comparing the changes in the electrical properties of the Cu devices with the changes in the electrical properties of the W devices, the extrinsic Cu diffusion effect and intrinsic SR-driven doping effect on the electrical properties of a-IGZO could be separated. After post-fabrication annealing, the electrical conductivity of a-IGZO in the W devices increased with an increasing annealing temperature as a result of SR-driven doping. However, because Cu diffusion occurs simultaneously, the electrical conductivity of a-IGZO dynamically changed depending on the dominant Cu diffusion paths. Moreover, resistive switching (RS; reversible electrical breakdown) behavior was newly observed at the Cu devices after Cu diffusion, whereas the W devices only showed irreversible electrical breakdown regardless of the post-annealing conditions. RS behavior have been reported in extrinsic

Cu-doped amorphous oxides (e.g., a-Ta₂O₅,^[24] a-SiO₂,^[25,29] or a-WO₃^[30]). Unfortunately, the effects of the Cu distribution and structural location of Cu in amorphous oxides on RS behavior have not been a focus of previous research, even though Cu is the dominant origin of RS behavior. In this study, we demonstrate that the RS characteristics of Cu devices are altered according to the location of the dominant site of Cu in a-IGZO. Moreover, the changes in the density of states (DOS) in a-IGZO with respect to the site location of the Cu were calculated based on first-principles calculations using the Vienna ab initio simulation package.^[31,32] Changes in the microstructural characteristics and chemical composition of a-IGZO due to Cu diffusion were also investigated using transmission electron microscopy (TEM), secondary ion mass spectrometry (SIMS), X-ray photoelectron spectroscopy (XPS), and Auger electron spectroscopy (AES). Based on these systematic experimental procedures with computations, we suggest Cu diffusion mechanisms within a-IGZO. This dynamic Cu diffusion effect and the Cu diffusion kinetics in AOSs represent an unprecedented result and will enable researchers to design and tailor extrinsic metal-doped AOSs subjected to solid-state electrochemical devices such as RS memories.

2. Results and Discussion

2.1. Changes in *I*–*V* Characteristics

Figure 1b shows the semilogarithmic *I*–*V* curves of the devices (contact area of 25 μm²) in the as-fabricated state measured at room temperature (RT). Voltage was applied to the TE, whereas the BE was grounded. Initially, both devices showed asymmetric *I*–*V* curves and the electrical conductance (*G*) of the W devices was higher than that of the Cu devices. The rectifying behavior indicates that electrical conduction of the as-fabricated devices is affected by the Schottky barrier at the metal/a-IGZO interface rather than the bulk resistance of a-IGZO.^[33] Because *G* is higher under a negative bias than under a positive bias, the Schottky barrier height (Φ_B) at the a-IGZO/BE interface is higher than that at the a-IGZO/TE interface (Figure S1b, Supporting Information). Ideally, the difference in Φ_B between both interfaces should be negligible because the W devices are symmetric in structure or the work function difference between W (4.55 eV) and Cu (4.65 eV) is small for the Cu devices.^[34] These phenomena would be induced that the defects at the TE/a-IGZO interfaces, such as reduction in the a-IGZO surface (i.e., increase in the *V*_O concentration) in the vacuum chamber before TE deposition and/or TE material bombardment-induced changes in the chemical states of the a-IGZO elements (Figure S1c, Supporting Information), are generated during TE deposition.^[28,35] These interface states enhances the barrier tunneling conduction and consequently decrease the effective Φ_B at the TE interface.^[28,35] Because the initial free electron concentration in a-IGZO in the devices is below 10¹⁶ cm⁻³, the dominant conduction mechanism of the devices is Schottky thermionic emission.^[28,35] Schottky diode parameters, Φ_B , ideality factor (*n*), and series resistance (*R*_S) were extracted based on thermionic theory. Details of the estimation are provided in Figure S1 of the Supporting Information.^[28,35] The Φ_B and

n values of the W devices are similar to the values of the Cu devices, whereas the *R*_S of the former devices is smaller. *R*_S is the summation of the contact resistance at the TE/a-IGZO interfaces (*R*_C) and the bulk resistance of the undepleted region in a-IGZO thin-film patches (*R*_{Bulk}) as depicted in Figure S1d (Supporting Information).^[33] During the TE deposition, no diffusion of W and Cu occurred in the a-IGZO bulk.^[15,28] Thus, the discrepancy of *R*_S between W and Cu devices was strongly induced by the difference in *R*_C. Furthermore, these results indicate that the properties of the Schottky contact at the a-IGZO/BE interfaces are similar for the two devices, whereas the lower *R*_C values in the W devices relative to the Cu devices induce higher relative *G* of the W devices.

Figure 1c presents a map of the *I*–*V* curves of the devices with respect to the postfabrication annealing conditions, in which the temperature was varied from 300 to 500 °C for 1 to 100 h at maximum. *G* of the devices at ±1 V is presented in Figure 1d. After annealing at 300 °C for 1 h, *G* of both devices increased compared with that in the as-fabricated state. The rectifying characteristics were maintained after annealing for 100 h. Interestingly, *G* of the Cu devices increased with increasing annealing time, whereas that of the W devices remained relatively unchanged after an annealing time of 9 h. Note that *G* of the W devices decreased between an annealing time of 4 and 9 h, which would be induced in the increase of *R*_S as shown in Figure S1f (further details of this deduction are included in the Supporting Information). As the annealing temperature increased to 400 °C for 1 h, *G* of both devices increased further. *G* of the W devices showed a weak dependence on the annealing time while maintaining the rectifying behavior after annealing for 25 h. For the Cu devices, *G* was comparable (or slightly higher) than that of the W devices until an annealing time of 9 h. However, after annealing for 16 h, *G* of the Cu devices became lower than that of the W devices and exhibited symmetric *I*–*V* curves with significantly wider deviations of *G* among each device. After annealing at 500 °C for 1 h, *G* of the Cu devices decreased further, *G* of the W devices increased further and the *I*–*V* curves of the W devices became symmetric.

We previously reported that the origin of the annealing temperature-dependent increase in *G* of the W devices is SR-driven electron doping.^[28] As the annealing temperature increases, *N*_D increases because of the densification of a-IGZO due to SR. A plausible mechanism for these phenomena is that the *V*_{OS} in the deep donor or electron traps transform into *V*_{OS} in the shallow-donor state by free-volume reduction.^[36,37] From comparison of the *I*–*V* characteristics of the Cu devices with that of the W devices, the dominant role of Cu in a-IGZO can be determined as follows. (i) At 300 °C, the Cu increases the electrical conductivity of a-IGZO according to the diffusion time. (ii) At 400 °C, the dominant role of the Cu in a-IGZO is altered from increasing to decreasing the electrical conductivity with respect to the annealing time. (iii) At 500 °C, the Cu decreases the electrical conductivity of a-IGZO, even after an annealing time of 1 h. To analyze the Cu diffusion effect in detail, the conduction mechanism changes in the devices were analyzed as shown in Figure 1e, and Figures S2 and S3 (Supporting Information).

Figure 1e presents the variations in Φ_B and *n* with regard to the annealing conditions. After annealing at 300 °C, the

values of Φ_B and n of the Cu devices were similar to those of the W devices until an annealing time of 4 h. However, with a longer annealing time, Φ_B decreased and n increased for the Cu devices, whereas the W devices showed nearly constant values. The decrease in Φ_B with increasing n implies that N_D in a-IGZO increases.^[35] N_D in Schottky conducting devices can be quantified by analyzing the reverse leakage current,^[28,33] and the extracted values of N_D are shown at the top of Figure 1e. The details of the extraction methods and the accuracy of the values are elucidated in Figure S2 (Supporting Information) as well as our previous report.^[28] As the annealing time increased from 1 to 100 h, N_D in the Cu devices increased from $\approx 10^{16}$ to $\approx 10^{17}$ cm⁻³, whereas N_D in the W devices remained nearly unchanged ($\approx 10^{16}$ cm⁻³). These results suggest that the Cu dopant acts as an electron donor under diffusion conditions of 300 °C. N_D in the Cu devices significantly increased between annealing times of 4 and 9 h. Thus, the Cu dopant would arrive at the a-IGZO/BE interfaces (i.e., L of Cu is 40 nm) within an annealing time of 9 h. Therefore, D_{Cu} at 300 °C was extracted as $\approx 10^{15}$ cm² s⁻¹, and the estimated value is similar to the Cu diffusivity in several amorphous oxides.^[22–24]

After annealing at 400 °C for 1 h, N_D in the Cu devices increased to 10^{17} cm⁻³ which was higher than that in the W devices. Thus, Cu reaches the a-IGZO/BE interface within an annealing time of 1 h, and D_{Cu} at 400 °C was extracted as $\approx 10^{14}$ cm² s⁻¹. Based on D_{Cu} at 300 and 400 °C, the activation energy for D_{Cu} was roughly estimated as 0.9–1.2 eV, which is similar to the activation energy for Cu diffusion in SiO₂.^[22,23] Notably, N_D in the Cu devices remained nearly unchanged for up to 9 h and these values were similar to the N_D in the annealed Cu devices at 300 °C for 100 h. These results indicate that the solubility limit of donor-state Cu in a-IGZO is $\approx 10^{17}$ cm⁻³ at RT. Under annealing at 400 °C, Cu diffuses into a-IGZO enough to saturate the solubility limit of the donor-state Cu within annealing time of 1 h, whereas an annealing time of over 100 h is needed at 300 °C. After annealing for 16 h, N_D in the Cu devices could not be measured by thermionic emission theory because the Cu devices do not exhibit rectifying behavior. On the other hand, N_D in the W devices increased to $\approx 10^{17}$ cm⁻³ after annealing for 4 h due to SR-driven doping, and the values are nearly constant until 25 h.

After annealing at 500 °C, both the W and Cu devices showed symmetric I - V curves. However, G of the W devices further increased, whereas that of the Cu devices further decreased. The alteration of the I - V shapes of the W devices from asymmetric to symmetric indicates that the dominant conduction mechanism changed from thermionic emission to Pool-Frenkel (P-F) conduction (Figure S3a–c, Supporting Information).^[28] However, the I - V characteristics of the Cu devices were not fitted well by the orthodox P-F conduction theory (Figure S3d,e, Supporting Information). Tunneling-based conduction is also not the dominant conduction mechanism because G of the Cu devices was altered by the substrate temperature (Figure S3f, Supporting Information). Therefore, complex conduction mechanisms exist in the Cu devices that exhibit symmetric I - V curves.

The changes in the I - V characteristics of the Cu devices unprecedentedly suggest that Cu in a-IGZO not only acts as an electron donor but also decreases the electrical conductivity of

a-IGZO determined by the annealing temperature and time. In addition to the changes in the electrical conduction properties of the devices, the electrical breakdown characteristics with respect to the Cu doping conditions were investigated as shown below.

2.2. Electrical Breakdown Behavior

Figure 2a presents the typical electrical breakdown characteristics of the 25 μm^2 Cu devices after annealing at 300 °C. First, positive voltage is swept on the Cu devices until reaching a current value of 1 mA (i.e., compliance current, I_{CC}). In the as-fabricated state, the current drastically increased under a voltage of ≈ 7 V, which is called electroforming.^[38] When a voltage with the same polarity side is swept again without the limit of the I_{CC} , the Cu devices exhibited hard breakdown (HDBR) behavior (i.e., irreversible increase in G). After annealing for 9 h, the HDBR still occurred for the Cu devices. However, when the annealing time exceeded 16 h, the Cu devices exhibited RS behavior. According to the applied bias conditions, the low resistance state (LRS) of the Cu devices reversibly changes to the high resistance state (HRS). In contrast to the Cu devices, the W devices exhibit HDBR behavior regardless of the annealing time (Figure 2b; Figure S4a, Supporting Information). The breakdown voltage in the Cu devices decreased as the annealing time increased, whereas the values in the W devices remained relatively constant as shown in Figure 3c. These results indicate that the donor-state Cu dopant is the origin of the RS behavior in the Cu devices. An unipolar RS mechanism (i.e., occurrence of RS at the same bias polarity) was proposed, stating that the formation and rupture of conductive filaments (CFs) consist of mobile ions, interconnecting the TE and BE.^[38,39] During unipolar RS, the CFs are partially melted by Joule-heating (RESET) and restored by mobile ions (SET).^[38,40] Thus, the Cu ions in a-IGZO electrochemically migrate and help form/rejuvenate the CFs. Without extrinsic Cu doping, a-IGZO can exhibit CF-based RS governed by intrinsic V_O migration (previous studies of a-IGZO RS devices are summarized in Table S1, Supporting Information). The initial V_O concentration and distribution in the a-IGZO bulk significantly affected the emergence/characteristics of RS.^[41–43] The interfacial reduction reactions of a-IGZO using Ti or Al electrodes, which can uptake O from a-IGZO (i.e., the generation of V_O s at the a-IGZO interfaces), are effective for the occurrence of RS.^[41] Thus, the HDBR of the W devices indicates that the concentration and distribution of V_O in a-IGZO were not sufficient to generate RS, regardless of post-fabrication annealing.

Figure 2c shows dependence of the resistance of the Cu devices on the contact area after annealing for 100 h. In addition to 25 μm^2 devices, 4–2500 μm^2 devices also exhibited RS behavior. The resistance at the LRS is independent of the contact area, whereas the resistance at the HRS, as well as the initial state, decreases as the contact area increases. These results support the occurrence of RS at the CFs, rather than homogeneous RS.^[44–46] At the HRS, the resistance of the Cu devices is dominated by the bulk resistance of a-IGZO, which corresponds to the ruptured region of the CFs, resulting in contact area dependent-resistance.^[43,44] Figure 2d shows the

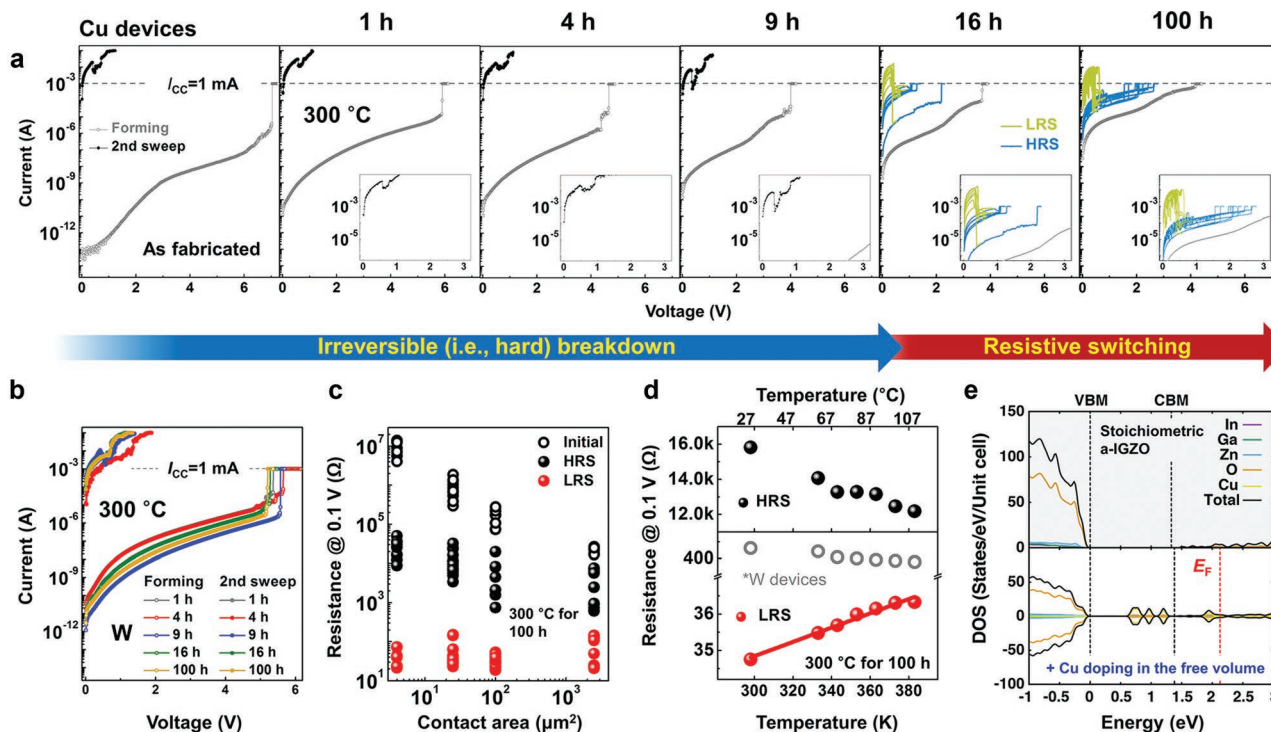


Figure 2. Electrical breakdown characteristics. a) The $25 \mu\text{m}^2$ Cu devices exhibited a hard breakdown in the as-fabricated state and after annealing at $300 \text{ }^\circ\text{C}$ for up to 9 h. However, unipolar RS behavior was observed after annealing for 16 h. b) The W devices after annealing at $300 \text{ }^\circ\text{C}$ solely showed hard breakdown regardless of the annealing time. c) Contact area and d) temperature dependence of the resistance (at 0.1 V) of the Cu devices after annealing at $300 \text{ }^\circ\text{C}$ for 100 h. The resistance of the electrically broken W devices with respect to the substrate temperature is also included. e) The DOS changes in stoichiometric a-IGZO due to Cu doping in the free volume.

temperature dependence of the resistance of the Cu and W devices annealed at $300 \text{ }^\circ\text{C}$ for 100 h after breakdown at an I_{CC} of 1 mA. The resistance of the Cu devices at the LRS linearly increased with increasing temperature, whereas that of the W devices decreased. Thus, the resistance of the Cu devices at the LRS exhibits metallic characteristics, whereas the conductive paths in the W devices have semiconducting characteristics.^[43,44] The absolute resistance of the Cu devices after breakdown were lower than that of the W devices (Figure S4c, Supporting Information), although the breakdown voltage of the W devices was higher than that of the Cu devices (Figure 3c). In general, the resistance of CFs is inversely proportional to the breakdown voltage (i.e., breakdown power).^[47] Thus, these results suggest that Cu is the main component of metallic CFs in the Cu devices, whereas the semiconducting conductive paths in the W devices are composed of intrinsic defects such as V_{O} s, which exhibit higher resistance than metallic CFs.^[44,48] The resistance of the Cu devices at the HRS is negatively dependent on the substrate temperature, which corresponds to the semiconducting behavior of the Cu devices at the HRS.^[44,45] The temperature coefficient of resistance (TCR) at the LRS equals $0.6 \times 10^{-3} \text{ K}^{-1}$, which is lower than the TCR of pure Cu nanowire ($2.5 \times 10^{-3} \text{ K}^{-1}$),^[49] which indicates that weak metallic CFs composed of Cu and other defects (V_{O} s) are formed in a-IGZO.^[50]

Because Cu ions are mobile, the Cu in a-IGZO is located in the free volume rather than the substitutional sites.^[18,21] Moreover, the Cu ions located in the free volume would act

as electron donors ($\text{Cu} \rightarrow \text{Cu}^{n+} + n\text{e}^-$, $n = 1, 2$), similar to the interstitial Cu in crystalline semiconductors.^[17,18] This statement is supported by first-principles calculations results; the Fermi level (E_{F}) lies above the conduction band minimum (CBM) when Cu is introduced into the free volume, as can be seen in Figure 2e, while substituting Cu in In, Ga, or Zn sites generated empty levels in the band gap (Figure S5, Supporting Information).

Therefore, the I - V characteristics changes and electrical breakdown behavior in the annealed devices at $300 \text{ }^\circ\text{C}$, along with the DOS computation results, strongly suggest that diffused Cu at $300 \text{ }^\circ\text{C}$ is dominantly located in the free volume in a-IGZO and acts as a mobile electron donor. Notably, when the annealing time was shorter than 16 h, the Cu devices exhibited HDBR, meaning that the Cu doping concentration and distribution in a-IGZO at the corresponding annealing time was not sufficient to form stable CFs during the voltage sweep at RT. Therefore, the Cu diffusion conditions determine the generation of RS and may affect the RS characteristics in a-IGZO. Alternation of the RS characteristics with respect to the Cu diffusion conditions, as well as the operating bias conditions, was further investigated as described below.

2.3. RS Characteristics

Figure 3a presents the RS characteristics of the $4 \mu\text{m}^2$ Cu devices after annealing at $400 \text{ }^\circ\text{C}$ for 1 h and 16 h with respect

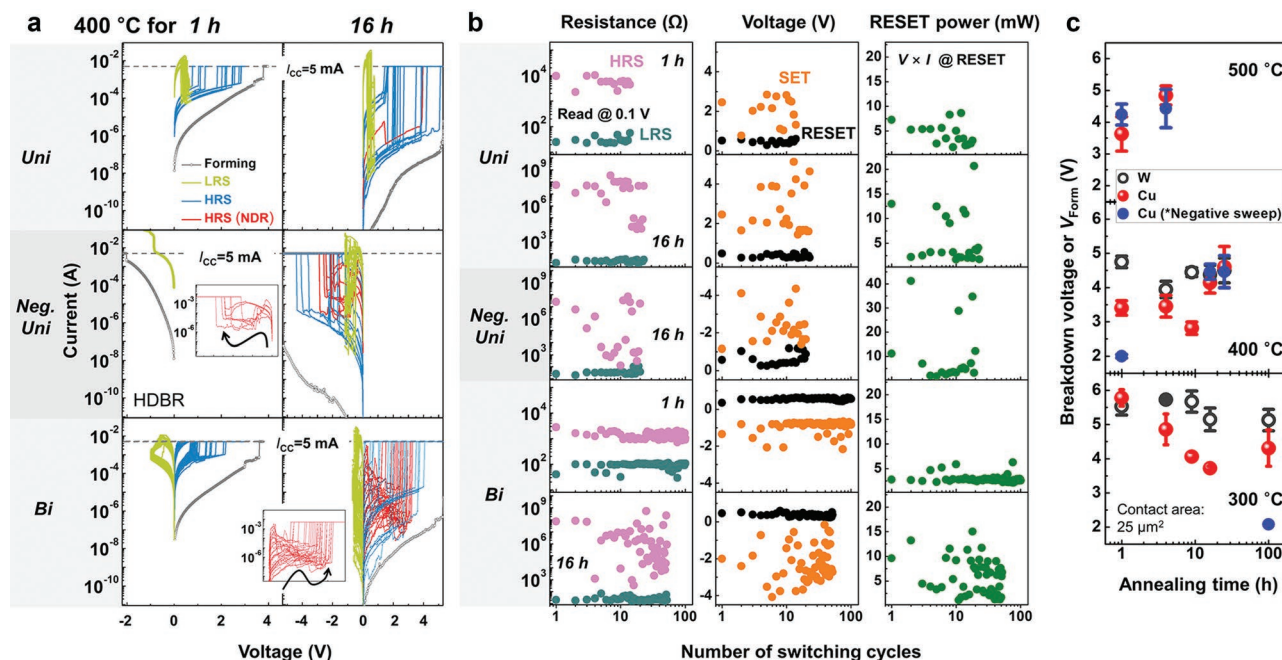


Figure 3. RS characteristics dependent on the Cu diffusion conditions. a) RS in the $4 \mu\text{m}^2$ Cu devices after annealing at $400 \text{ }^\circ\text{C}$ for 1 and 16 h with respect to the operating bias polarity (unipolar, negative-unipolar, and bipolar) and b) variation of the resistance at the LRS/HRS, SET/RESET voltage, and RESET power of the corresponding Cu devices with respect to the number of switching cycles. c) Breakdown voltage of the Cu devices and W devices with respect to the annealing conditions.

to an operating bias polarity. In addition to the unipolar bias condition, negative unipolar bias, and bipolar bias (i.e., SET under positive bias and RESET under negative bias) conditions were applied to operate the RS of the Cu devices. Moreover, the RS performances (resistance, voltage, and RESET power) of the corresponding Cu devices with respect to the number of switching cycles are presented in Figure 3b. The cumulative distribution of the RS performances of the Cu devices is also shown in Figure S6 (Supporting Information).

At an annealing condition of $400 \text{ }^\circ\text{C}$, an annealing time of 1 h was sufficient to generate unipolar RS in the Cu devices (top of Figure 3a), whereas the W devices exhibited HDBR regardless of the annealing time (Figure S4d, Supporting Information). These results are consistent with the donor-state Cu in the free volume becoming saturated at a-IGZO within an annealing time of 1 h at $400 \text{ }^\circ\text{C}$, which was sufficient for RS to occur (Figure 1e). The I_{CC} was 5 mA because G of both the Cu and W devices was too high to be broken under 1 mA. The forming voltage (V_{FORM}) was more reduced than that of V_{FORM} in the Cu devices annealed at $300 \text{ }^\circ\text{C}$ (Figure S4e, Supporting Information and Figure 3c). CF formation is affected by the redox rate of Cu ions as well as Cu ion mobility.^[25] Thus, higher G may increase the reduction rate of Cu ions, and CFs are consequently formed at lower voltage. After annealing for 16 h, unipolar RS occurred, and positive TCR values at LRS were observed (Figure S4f, Supporting Information), implying that, although the dominant role of the Cu dopant was to reduce the electrical conductivity of a-IGZO, enough mobile Cu still existed in a-IGZO to form metallic CFs, generating unipolar RS. The V_{FORM} of the Cu devices annealed for 16 h was higher than that of the Cu devices annealed for 1 h, which was

induced by the decrease in the CF formation rate due to low G . Compared to the Cu devices annealed for 1 h, the deviation of the resistance values at the HRS was greater, although that of the LRS was similar (top of Figure 3b). Moreover, the distribution of the switching voltage was wider, and a higher RESET power consumption was observed. These results mean that the CFs were more randomly ruptured and the conduction paths at the HRS became more irregular than in the devices annealed for 1 h. Therefore, Cu-related defects, which decrease the electrical conductivity of a-IGZO, are involved in CFs formation/rupture and deterioration of unipolar RS performance.

When negative bias was applied for unipolar RS, the devices annealed for 1 h exhibited HDBR (middle of Figure 3a), which would be induced by a reduction in the contribution of Cu on CF formation because Cu ions in a-IGZO drift to the Cu electrodes (i.e., backward Cu migration) and the electrochemical dissolution of Cu ions from the Cu TE is suppressed by the application of negative bias.^[25,29,45] However, the devices annealed for 16 h exhibited negative unipolar RS behavior, although the RESET power consumption still fluctuated with poor switching uniformity. These results suggest that Cu-related defects supply enough Cu ions exhibit RS under negative bias. Conversely, Cu-related defects act as indiscriminate Cu ion sources, causing poorer RS uniformity than a-IGZO which dominantly contains donor-state Cu.

In addition to unipolar RS, the Cu devices annealed for 1 and 16 h exhibited bipolar RS, and the RS endurance was enhanced (bottom of Figure 3a,b). This behavior would be induced by the alternating polarity of the bias. Under positive unipolar RS, the Cu ions from the Cu TE continuously migrate into a-IGZO regardless of the SET/RESET from electrochemical

dissolution.^[29] On the other hand, the mobile Cu concentration in a-IGZO continuously decreases due to backward migration as well as the suppression of electrochemical dissolution of Cu TE under negative unipolar RS. Thus, positive unipolar bias and negative bias conditions induce an excess or deficient concentration of donor-state Cu in a-IGZO, respectively, and cause deterioration of the RS endurance. However, under bipolar bias conditions, the Cu concentration in a-IGZO attempts to maintain itself under the repetitive alternation of the direction of Cu migration, and hence, the RS endurance is improved. A bipolar bias condition also enhanced switching uniformity of the devices annealed for 1 h compared to the positive unipolar bias condition. However, the switching uniformity of the devices annealed for 16 h was not enhanced. Interestingly, the devices annealed for 16 h exhibited significant negative differential resistance (NDR) behavior, a decrease in current with increasing voltage, with SET processes. The origin of the voltage-controlled NDR behavior has been suggested to be the space charge field in active materials.^[33,51] During voltage application, the charge density in the space charge region increases because of charge trapping, and the space charge field increases, which opposes the direction of the current, resulting in a decreased current.^[51] Thus, Cu-related defects would act as charge-trapping sites in addition to Cu ion sources. Although subsequent rupturing of residual CFs by Joule heating could also affect the NDR behavior at HRS,^[52] the NDR behavior frequently occurs under bipolar conditions rather than under unipolar bias conditions. The charge density in the space charge region due to Cu-related defects is significantly altered during the application of bipolar bias rather than unipolar bias conditions, whereas Joule heating is affected by the magnitude of the current density, not the bias polarity. Therefore, the Cu-related defect-induced space charge region would be the dominant origin of NDR behavior. When properties of the CFs (length, width, or distribution) are changed by electrochemical Cu migration, the charge density in the space charge region concurrently fluctuates, resulting in deterioration of the RS performance. Therefore, suppression of the formation of Cu-related defects is a prerequisite for highly uniform RS in Cu-doped a-IGZO.

In addition to the Cu devices annealed at 400 °C for 1 and 16 h, the RS performances of the Cu devices after annealing at 300 °C for 100 h and at 500 °C for 1 h are also included in Figure S6 (Supporting Information). The RS performances of the devices annealed at 300 °C for 100 h and at 500 °C for 1 h were similar to the performances of the devices annealed at 400 °C for 1 and 16 h, respectively. Thus, RS performance is strongly affected by the dominant role of Cu, either as an electron donor or through the formation of a space charge region in the bulk a-IGZO. The current reported RS performance of Cu devices is still insufficient for commercialization as memristive devices, and the more elaborated estimation of the RS performance (e.g., retention, pulse switching mode) is required.^[38,40] However, we believe that RS performance could be enhanced through optimization of the doping concentration and distributions of the donor-state Cu, as well as the bulk properties of a-IGZO with suppressed formation of Cu-related defects.

Two remarkable findings of this study are that Cu diffusion enables AOSs to possess RS characteristics and that RS properties are determined by the dominant electronic states of the

Cu, which are altered by the thermal history. After annealing at 300 °C, the mobile Cu donor is dominant even after annealing for 100 h. However, the Cu-related defects that form the space charge region in a-IGZO are dominant after annealing at 500 °C for 1 h. At 400 °C, the dominant role of the Cu is altered according to the annealing time. The origin of the alternation of the dominant role of the Cu in a-IGZO based on microscopic and compositional analysis of the Cu distribution in a-IGZO is discussed in-depth below.

2.4. Microstructure and Chemical Composition Analysis

Figure 4a shows the cross-sectional images of the devices measured by high-angle annular dark-field scanning transmission electron microscopy (HAADF-STEM) and high-resolution TEM (HRTEM) with respect to the annealing conditions. After annealing at 400 °C for 1 h, Cu was not detected in a-IGZO by energy dispersive X-ray spectroscopy (EDS). Moreover, the amorphous phase was maintained, as determined by the HRTEM images and fast Fourier transform (FFT) diffractogram of the white-square regions (additional images are shown in Figure S8, Supporting Information). Although donor-state Cu diffuses into a-IGZO, the Cu doping concentration is $\approx 10^{17} \text{ cm}^{-3}$ (Figure 1e), which is far below the EDS detection limits ($\approx 10^{20} \text{ cm}^{-3}$).^[53] Interestingly, as the annealing time increased to 16 h, Cu-rich clusters formed in a-IGZO. As the annealing temperature increased to 500 °C, the Cu-rich clusters were also detected after 1 h, whereas interdiffusion did not occur in the W devices with maintenance of the amorphous phase. In addition to Figure 4a, additional EDS results are shown in Figures S9–S13 (Supporting Information). The spatial distribution and size of the Cu-rich clusters were nonuniform. Notably, Figure 4b shows that In concentration was relatively higher at the location of the Cu-rich clusters (EDS line profiles #2, 3, and 4) than in the bulk a-IGZO, which severely decreased compared to Ga or Zn (line profile #1). Additional EDS maps and line profiles show similar phenomena, although some results demonstrate that only Cu agglomerated without In inclusion (line profile #5 in Figure 4b; Figures S11 and S13, Supporting Information). Thus, the Cu-rich clusters tend to contain In rather than Ga or Zn, whereas a-IGZO become In-deficient. The Cu-rich clusters are crystalline as shown in the HRTEM images and FFT diffractograms (Figure 4c). Additional images are presented in Figures S14–S23 (Supporting Information). Based on the EDS results, possible candidates of the crystalline phases of the Cu-rich clusters include pure Cu, Cu oxides, Cu–In intermetallic compounds or In-doped Cu oxides. Among these candidates, $\text{Cu}_2\text{In}_2\text{O}_5$, CuO, and CuInO_2 (Figure S16, Supporting Information) were identified. Interestingly, $\text{Cu}_{10}\text{In}_7$, a Cu–In intermetallic compound was also identified. Cu–In intermetallic clusters would act as indiscriminate Cu ion sources that affect CF formation/rupture,^[25] resulting in the degradation of RS performances. However, Cu–In intermetallic compounds are not the dominant crystalline phases of the Cu-rich clusters for the following reasons. If Cu–In intermetallic compounds are distributed in a-IGZO similar to the EDS map results, a highly conducting ohmic behavior would be observed in the devices because the spatial gaps

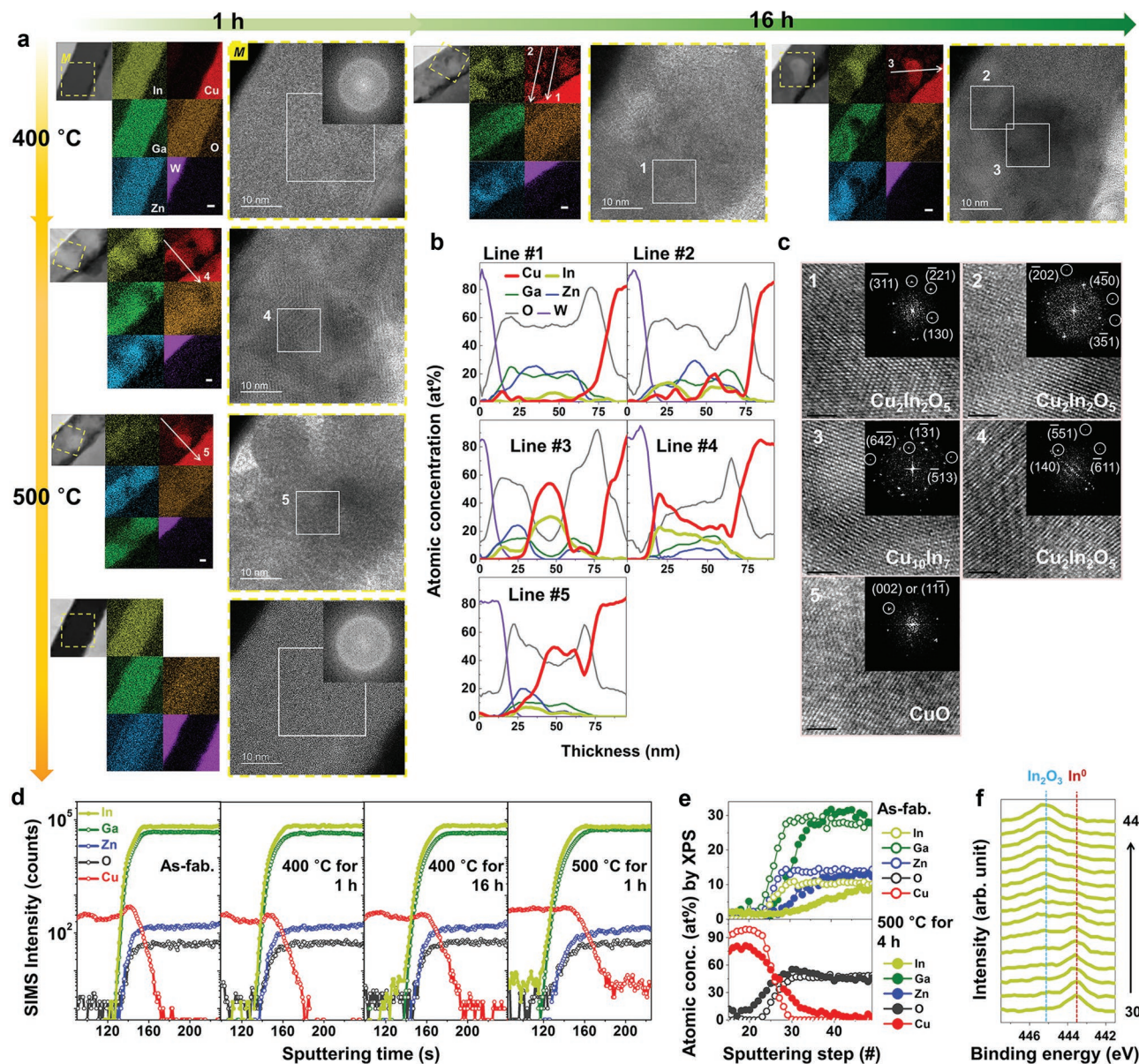


Figure 4. Microstructural and chemical composition analysis. a) HAADF-STEM images, EDS maps, and HRTEM images of the devices with respect to the annealing conditions. Scale bar: 10 nm. The location of the HRTEM images is marked in the HAADF-STEM images as a yellow-dotted square (M). b) EDS line profiles in the HAADF-STEM images and c) FFT diffractograms of selected areas in the HRTEM images of (a). Scale bar: 2 nm. d) SIMS and e) XPS analyses of the Cu/a-IGZO interfaces with respect to the annealing conditions. The SIMS and XPS analyses were conducted on multilayer thin films composed of Cu/a-IGZO thin-film stacks, not at the device level. f) In $3d_{5/2}$ spectra after annealing at 500 °C for 4 h with respect to the sputtering step from 30 to 44.

among the Cu-rich clusters and electrodes are narrow enough to form ohmic conduction paths.^[33,54] Therefore, low G of the Cu devices (Figure S7, Supporting Information) indicates that the dominant crystalline phases of the Cu-rich clusters are not Cu–In intermetallic compounds, but rather In-doped Cu oxide clusters which exhibit p-type and low electrical conductivity.^[5,55]

Some of FFT diffractions could be not analyzed because Moiré fringes, which are induced by double diffraction in polycrystalline phases, hindered the identification of the crystalline phases of the Cu-rich clusters.^[56] However, the most important point is that In-doped Cu oxide clusters formed

bulk heterogeneous pn junctions in n-type a-IGZO. These nonuniform and nonorientable pn junctions would overlap with each other due to the narrow spatial gaps among clusters. Moreover, nanosized Cu–In metallic clusters would act as charge-trap sites.^[51,57] These findings strongly suggest that the space charge region in the pn junctions and nanosized traps are the microscopic origin of NDR behavior during RS^[33,51] and also induce the complex conduction mechanism of the Cu devices with low G . Moreover, these results may provide clues to determining the atomic origin of the amorphization-induced insulating properties of p-type crystalline Cu-based oxides.^[7]

When amorphization occurs, Cu-based metallic clusters or pn junctions (e.g., Cu₁₀In₇ or p-type Cu₂O/n-type In₂O₃ in CuInO₂) may form in the short-range ordering in amounts that are sufficiently low to not be detected by X-ray diffraction analysis,^[7] decreasing the electrical conductivity to insulating ranges, whereas the Cu in the free volume is relatively negligible.

For a more macroscopic and precise quantification analysis of the changes in the composition profiles, SIMS analysis was conducted on Cu/a-IGZO thin films, as shown in Figure 4d (details of SIMS results are presented in Figure S24, Supporting Information). The analysis area and detection limit of SIMS were $\approx 10^4 \mu\text{m}^2$ and $\approx 10^{18} \text{cm}^{-3}$, respectively.^[58] After annealing at 400 °C for 1 h, the compositional profiles were nearly unchanged. However, when the annealing time was 16 h, Cu was clearly detected in the a-IGZO. At the same time, In diffused into the Cu thin films, whereas the composition profiles of Ga, Zn, and O remained nearly constant. As the annealing temperature increased to 500 °C for 1 h, severe interdiffusion of Cu and In occurred.

The changes in the composition profiles of the Cu/a-IGZO thin films after annealing at 500 °C for 4 h, as measured by XPS, also show that the In concentration in a-IGZO severely decreased compared to the concentrations of Ga or Zn and that In had diffused into Cu thin films, as presented in Figure 4e and Figure S25 (Supporting Information). AES analysis also presents similar results with XPS (Figure S29, Supporting Information). Therefore, In provides the most dominant substitutional diffusion site for Cu in a-IGZO. In is the core element forming the CBM in a-IGZO.^[9,59,60] Therefore, a decrease in the In concentration also causes a reduction in the electrical conductivity of a-IGZO, in addition to the formation of Cu–In–O clusters.

The TEM, SIMS, XPS, and AES results may raise doubt as to how Cu–In–O clusters are formed in a-IGZO, whereas In becomes severely deficient in a-IGZO because of the substitutional Cu doping. This suspicion could be resolved by elucidation of the Cu diffusion behavior in a-IGZO with respect to the annealing temperature as follows. Figure 5a depicts the composition profile changes with respect to the dominant Cu diffusion paths. At the Cu/a-IGZO interfaces, a concentration gradient (i.e., chemical potential gradient) of elements exists (Table S2, Supporting Information). The Cu solubility at the substitutional sites (S_{sub}) would be higher than the Cu solubility in the free volume (S_{free}) because the Cu in the free volume was not detected by EDS and SIMS, whereas substitutional Cu was observed (Figure 4a,d). As noted above, two paths (free volume and substitutional sites) are available for Cu diffusion in a-IGZO. Figure 5b depicts the potential energy band diagram of Cu diffusion in terms of the diffusion paths. Diffusion through the free volume in amorphous materials resembles the interstitial diffusion in crystalline materials.^[21] To attain Cu diffusion through the free volume, Cu must exceed the Gibbs free energy for migration to the other site in the free volume (ΔG_{m}). In the case of substitutional Cu diffusion, however, vacant cation sites are needed in addition to enough thermal energy to overcome ΔG_{m} .^[21] Thus, the activation energy of substitutional diffusion is the summation of ΔG_{m} and ΔG_{f} , where ΔG_{f} is the Gibbs free energy of cation vacancy formation in a-IGZO.^[21] Therefore, free volume diffusion is likely faster than substitutional

diffusion^[17,21] and the Cu in the free volume (Cu_{f}) dominated the electrical properties of a-IGZO in the early stage of diffusion (left of Figure 5a). However, with further annealing, the diffusion of substitutional Cu (Cu_{s}) utilizing the In sites became dominant, while the concentration of Cu_{f} became saturated (middle of Figure 5a). Substitutional Cu doping would occur in two ways, jumping of pre-existing cation vacancies in a-IGZO and a “kick-out” reaction in which Cu_{f} pushes the cations in the a-IGZO matrix, resulting in cations in the free volume.^[61] For n-type oxide semiconductors, the concentration of pre-existing cation vacancies (i.e., p-type defects) is negligible small.^[3] Therefore, the “kick-out” reaction would be the dominant mechanism for substitutional Cu diffusion, and In in the free volume (In_{f}) is formed as depicted in Figure 5c. XPS results showed that metallic In was newly detected in the Cu-doped a-IGZO bulk after annealing at 500 °C (Figure 4f; Figures S26–S28, Supporting Information). These results support the formation of metallic In_{f} and Cu–In intermetallic clusters due to Cu diffusion. After annealing, the dissolved Cu became supersaturated as the ambient temperature decreased to RT. As a result, the supersaturated Cu and In_{f} formed the Cu–In–O clusters in the bulk a-IGZO (right of Figure 5a,c).

In general, dopants prefer to substitute the same valence cations in complex oxides.^[62] Moreover, the Zn–O bond energies in a-IGZO are weaker on average than those of Ga–O or In–O.^[63] According to these factors, Zn^{2+} may be the dominant substitutional site for the Cu^{2+} , contradictory to our results. To elucidate the origin of In^{3+} as the most preferred substitutional site for Cu, we considered the activation energy of substitutional diffusion as shown below. ΔG_{f} would be strongly related to the standard Gibbs free energy of oxide formation ($\Delta G_{\text{ox}}^{\circ}$) of In, Ga, or Zn because the In–O, Ga–O, or Zn–O bonds should be reduced (i.e., bond breaking) to form the substitutional sites. The probability of cation vacancy formation would increase as the absolute value of $\Delta G_{\text{ox}}^{\circ}$ decreased. In the range of 300–500 °C, the $|\Delta G_{\text{ox}}^{\circ}|$ of In is the lowest compared to that of Ga and Zn (see Figure S30, Supporting Information, e.g., $|\Delta G_{\text{ox}}^{\circ}|$ of In, Ga, and Zn is 4.9, 6.0, and 5.9 eV at 400 °C, respectively).^[64] A previous theoretical study also suggested that the In–O polyhedra in a-IGZO have a greater tendency to lose O than Ga–O or Zn–O.^[59] Therefore, we believe that In provides a substitutional site for Cu because In^{3+} is easily reduced compared to Ga^{3+} or Zn^{2+} in a-IGZO.

Figure 5d summarizes the Cu diffusion kinetics in a-IGZO. At low-temperature annealing (i.e., ≤ 300 °C), Cu hardly substitute In, Ga, or Zn due to a lack of thermal energy needed to overcome the activation energy of $\Delta G_{\text{m}} + \Delta G_{\text{f}}$. Instead of substitutional diffusion, Cu dominantly diffused into a-IGZO through the free volume. After annealing, most of the Cu was still located in the free volume, and the Cu–In–O clusters were negligible. The Cu_{f} acted as a mobile electron donor and generated CF-based RS. When the annealing temperature increased enough for substitutional Cu diffusion to occur, Cu dominantly substituted for In. Moreover, the Cu_{s} and In_{f} formed Cu–In–O crystalline clusters, In-doped Cu oxides and Cu–In intermetallic compounds, in a-IGZO after annealing. These clusters decreased the electrical conductivity and also deteriorated the RS performances as they formed space charge-fields in a-IGZO. We believe that this unprecedented dynamic Cu diffusion effect on the electrical

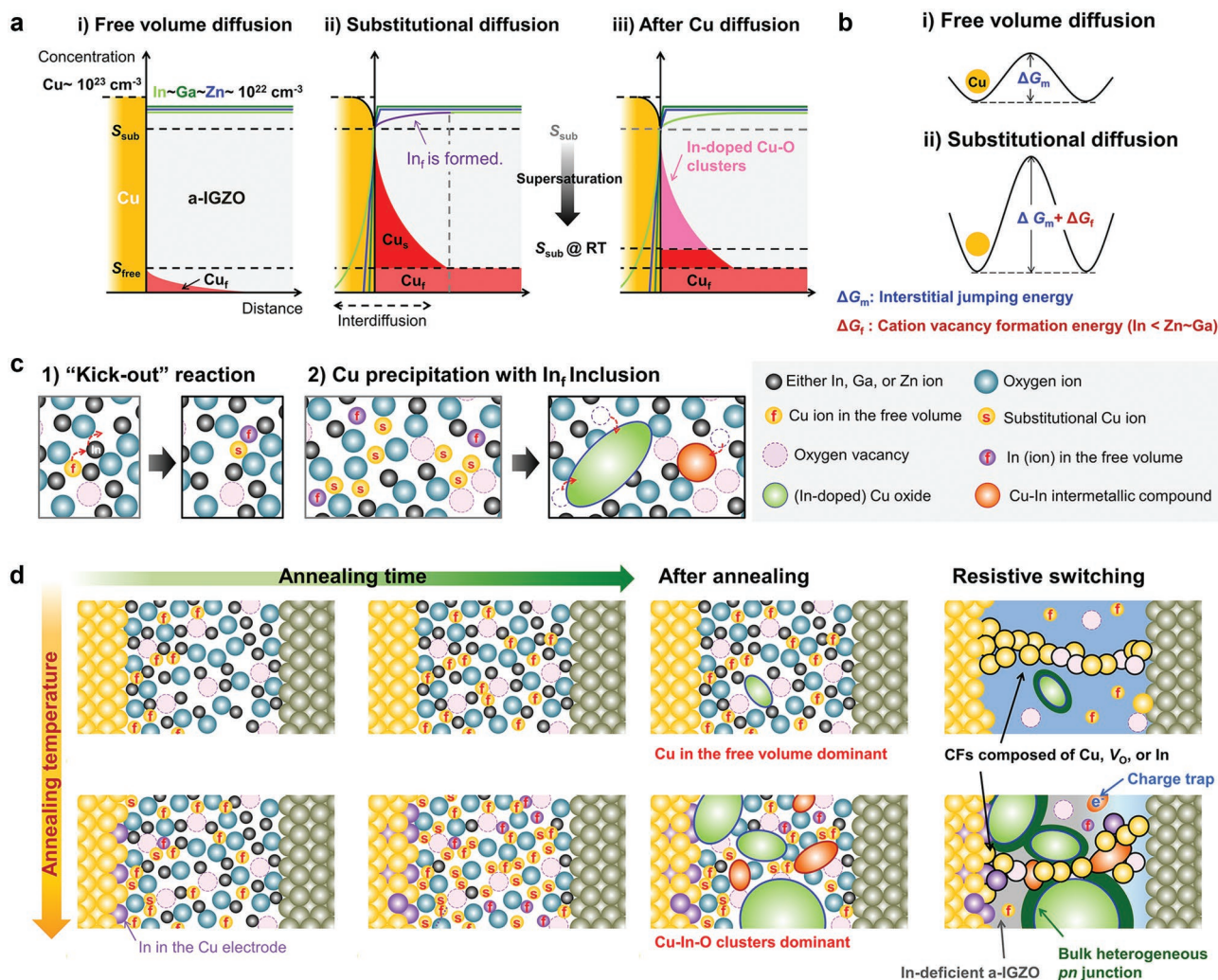


Figure 5. Cu diffusion kinetics in a-IGZO. Schematics of the a) composition profile changes in the Cu/a-IGZO contacts, b) potential energy diagram of Cu diffusion, and c,d) atomic movement in the Cu devices according to the diffusion conditions. In (c) and (d), a relative size variation of the elements due to the ionization (Table S3, Supporting Information) was considered. At low-temperature annealing (e.g., 300 °C), Cu dominantly diffuses in a-IGZO through the free volume and acted as an electron donor. At high-temperature annealing (e.g., 400 °C), substitutional Cu, which prefers In to Ga or Zn, becomes dominant as the annealing time increases. In in the free volume (In_f) is generated by a “kick-out” reaction in which Cu in the free volume pushes In in the a-IGZO matrix. After annealing, supersaturated Cu and In_f form Cu–In–O crystalline clusters, In-doped Cu oxides and Cu–In intermetallic compounds, in a-IGZO. Under application of the bias, the Cu in the free volume gave rise to CF-based RS, whereas bulk heterogeneous pn junctions due to In-doped Cu oxides and nanosized traps due to Cu–In intermetallics deteriorated the RS performance.

properties of a-IGZO will provide guidelines to design AOS-based RS devices through Cu diffusion and to understand the degradation of electrical performance in AOS electronics due to Cu contamination for the following reasons. First, the transition of the dominant diffusion site from the free volume to the substitutional sites can generally occur in AOSs with respect to the annealing temperature and time. Second, the dominant substitutional diffusion sites of Cu in AOSs would be strongly determined by the $|\Delta G_{\text{ox}}^{\text{c}}|$ of the cations in the AOSs. Third, the mobile Cu in the free volume gives rise to RS but can also cause undesired electrical breakdown in AOS electronics. Finally, suppression of Cu precipitates combined with substituted cations is prerequisite for the high performance of RS devices as well as AOS electronics because these precipitates form unpredictable space-charge regions in AOSs and/or act as indiscriminate Cu ion sources.

3. Conclusion

In conclusion, we revealed the Cu diffusion mechanism in a-IGZO and the dynamical changes in the effect of Cu on the electrical properties of a-IGZO. Cu diffusion occurs through two paths, free volume and substitutional sites. Because Cu diffusion in the free volume is faster than substitutional diffusion, Cu is dominantly located in the free volume in the early stage of annealing and has similar diffusivity as the Cu in a-SiO₂. The Cu in the free volume acts as a mobile electron donor and generates RS behavior as the origin of the CFs. As the annealing time elapses, substitutional Cu diffusion becomes predominant, which prefers In to Ga or Zn. After annealing, supersaturated Cu heterogeneously forms In-doped Cu oxide clusters and Cu–In intermetallic clusters in a-IGZO combined

with In_f . Because bulk-heterogeneous pn junctions and nano-sized traps are formed in a-IGZO with the reduction of the In concentration, the electrical conductivity of a-IGZO decreases. Moreover, these clusters induce NDR behavior in a-IGZO and deteriorate the performance of CF-based RS. To improve the RS performance, the formation of Cu–In–O clusters must be suppressed. Our results can be readily expanded to a universal Cu diffusion mechanism in AOSs and will enable researchers to develop RS devices based on Cu-doped AOSs.

4. Experimental Section

Device Fabrication and Electrical Measurements: For the BE of the devices, 100 nm thick W was deposited on n-type Si wafer using DC sputtering, which was passivated with a 300 nm thick SiN_x layer deposited by plasma-enhanced chemical vapor deposition at a substrate temperature of 300 °C. A SiN_x layer was patterned through the holes using photolithography and dry etching, and the area was varied from 4 to 2500 μm^2 . This step was followed by RF sputtering of 40 nm thick a-IGZO at RT. Details of the depositions condition of a-IGZO (initial free electron concentration in a-IGZO of below 10^{16} cm^{-3}) are presented in a previous report.^[28] The chemical composition of the deposited films had an atomic ratio of In:Ga:Zn = 1:1.6:0.8.^[28] The a-IGZO thin films were patterned into square-shaped patches; each of which area had an area of 6400 μm^2 to fill the SiN_x hole. The TE consisted of a Cu or W (100 nm thick)/Ta–Al (100 nm thick) pattern to cover the a-IGZO thin-film patches by DC sputtering followed by a lift-off process. The Ta–Al bilayer prevented interaction between a-IGZO and the ambient atmosphere (Figure S1a of the Supporting Information depicts the fabrication processes of the devices). The resultant devices were annealed at a temperature between 300 and 500 °C for up to 100 h under vacuum (10^{-6} Torr). After annealing, the I – V characteristics of the devices were measured using a 4156C semiconductor parameter analyzer (Agilent Technologies, Santa Clara, CA, USA) with variations of the substrate temperature from RT to 80 °C. The TCR in the devices after electrical breakdown was measured using a MIRA EM tester (Qualitau, Sunnyvale, CA, USA).

Analysis of the Microstructure and Chemical Composition: TEM analysis of the devices after annealing was conducted using a JEM-2100F transmission electron microscope (JEOL, Tokyo, Japan). The TEM samples were fabricated using a focused ion beam (SMI3050SE, SII NanoTechnology, Chiba, Japan). Composition maps were obtained by STEM-EDS. Time-of-flight SIMS (TOF.SIMS 5, ION-TOF GmbH, Münster, Germany) was utilized to measure the compositional changes in the multilayer films. XPS analysis (PHI-5000 Versa Probe, Physical Electronics, Chanhassen, MN, USA) and AES analysis (PHI-700 Auger Nanoprobe, ULVAC-PHI, Inc., Kanagawa, Japan) were also conducted on the multilayer films to measure the changes in the chemical states of In, Ga, Zn, O, and diffused Cu in a-IGZO, as well as the compositional profile changes after annealing.

Computation Details: The projector-augmented wave pseudopotentials^[65] and generalized gradient approximation (GGA)^[66] were used to determine the exchange-correlation energy. The orbital-dependent, on-site energy was employed for the metal (In, Ga, Zn, and Cu)- d electrons to correct the unphysical strong self-interaction of GGA.^[67,68] The amorphous structure of a-IGZO was modeled with stoichiometry of $n_{\text{In}}:n_{\text{Ga}}:n_{\text{Zn}} = 1:1:1$ and 18 formula units of InGaZnO_4 using a melt-quenching method via molecular dynamics (MD) simulations, employing the computational parameters from ref. [68]. The geometry of the final amorphous structure was fully optimized until the forces on each atom converged to 0.05 eV Å⁻¹ at 0 K using a 500 eV plane-wave cutoff energy and Γ point-only k-point sampling.

Supporting Information

Supporting Information is available from the Wiley Online Library or from the author.

Acknowledgements

This research was supported by the MOTIE (Ministry of Trade, Industry & Energy (10051601) and KDRC (Korea Display Research Corporation) support program for the development of future devices technology for display industry. This work was also supported by the National Research Foundation of Korea (NRF) grant funded by the Ministry of Science, ICT & Future Planning (MSIP) (Grant No. NRF 2015055406).

Keywords

amorphous oxide semiconductors, Cu diffusion, Cu doping, resistive switching, structural locations

Received: January 19, 2017

Revised: March 20, 2017

Published online: May 3, 2017

- [1] H. Kawazoe, M. Yasukawa, H. Hyodo, M. Kurita, H. Yanagi, H. Hosono, *Nature* **1997**, 389, 939.
- [2] S. Sheng, G. Fang, C. Li, S. Xu, X. Zhao, *Phys. Status Solidi A* **2006**, 203, 1891.
- [3] J. Robertson, S. J. Clark, *Phys. Rev. B* **2011**, 83, 075205.
- [4] Y. Kanai, *Jpn. J. Appl. Phys.* **1991**, 30, 703.
- [5] S. J. Wen, G. Couturier, G. Campet, J. Portier, J. Claverie, *Phys. Status Solidi A* **1992**, 130, 407.
- [6] H. L. Pan, B. Yao, T. Yang, Y. Xu, B. Y. Zhang, W. W. Liu, D. Z. Shen, *Appl. Phys. Lett.* **2010**, 97, 142101.
- [7] S. Narushima, H. Mizoguchi, K. Shimizu, K. Ueda, H. Ohta, M. Hirano, T. Kamiya, H. Hosono, *Adv. Mater.* **2003**, 15, 1409.
- [8] K. Nomura, H. Ohta, A. Takagi, T. Kamiya, M. Hirano, H. Hosono, *Nature* **2004**, 432, 488.
- [9] T. Kamiya, H. Hosono, *NPG Asia Mater.* **2010**, 2, 15.
- [10] J. Zhang, Y. Li, B. Zhang, H. Wang, Q. Xin, A. Song, *Nat. Commun.* **2015**, 6, 7561.
- [11] J. Yoon, Y. Jeong, H. Kim, S. Yoo, H. S. Jung, Y. Kim, Y. Hwang, Y. Hyun, W.-K. Hong, B. H. Lee, S.-H. Choa, H. C. Ko, *Nat. Commun.* **2016**, 7, 11477.
- [12] P. S. Yun, J. Koike, *J. Electrochem. Soc.* **2011**, 158, H1034.
- [13] J. Jeong, G. J. Lee, J. Kim, B. Choi, *Appl. Phys. Lett.* **2012**, 100, 112109.
- [14] Y. H. Tai, H. L. Chiu, L. S. Chou, *J. Electrochem. Soc.* **2012**, 159, J200.
- [15] J. R. Yim, S.-Y. Jung, H.-W. Yeon, J.-Y. Kwon, Y.-J. Lee, J.-H. Lee, Y.-C. Joo, *Jpn. J. Appl. Phys.* **2012**, 51, 011401.
- [16] C.-K. Lee, S. Y. Park, H. Y. Jung, C.-K. Lee, B.-G. Son, H. J. Kim, Y.-J. Lee, Y.-C. Joo, J. K. Jeong, *Phys. Status Solidi RRL* **2013**, 7, 196.
- [17] R. N. Hall, J. H. Racette, *J. Appl. Phys.* **1964**, 35, 379.
- [18] A. A. Istratov, E. R. Weber, *J. Electrochem. Soc.* **2002**, 149, G21.
- [19] H.-W. Yeon, S.-Y. Jung, J.-R. Lim, J. Pyun, H. Kim, D. Baek, Y.-C. Joo, *Electrochem. Solid-State Lett.* **2012**, 15, H157.
- [20] S. I. Kim, J.-S. Park, C. J. Kim, J. C. Park, I. Song, Y. S. Park, *J. Electrochem. Soc.* **2009**, 156, H184.
- [21] D. A. Porter, K. E. Easterling, *Phase Transformations in Metals and Alloys*, Chapman & Hall, London, UK **1992**.
- [22] J. D. McBrayer, R. M. Swanson, T. W. Sigmon, *J. Electrochem. Soc.* **1986**, 133, 1242.
- [23] Y. Shacham-Diamand, A. Dedhia, D. Hoffstetter, W. G. Oldham, *J. Electrochem. Soc.* **1993**, 140, 2427.
- [24] N. Banno, T. Sakamoto, N. Iguchi, H. Sunamura, K. Terabe, T. Hasegawa, M. Aono, *IEEE Trans. Electron Devices* **2008**, 55, 3283.
- [25] Y. Yang, P. Gao, L. Li, X. Pan, S. Tappertzhofen, S. Choi, R. Waser, I. Valov, W. Lu, *Nat. Commun.* **2014**, 5, 4232.

- [26] A. S. Lee, N. Rajagopalan, M. Le, B. H. Kim, H. M'Saad, J. *Electrochem. Soc.* **2004**, *151*, F7.
- [27] T. O. Yosi Shacham-Diamond, M. Datta, T. Ohba, *Advanced Nanoscale ULSI Interconnects: Fundamentals and Applications*, Springer-Verlag, New York **2009**.
- [28] H.-W. Yeon, S.-M. Lim, J.-K. Jung, H. Yoo, Y.-J. Lee, H.-Y. Kang, Y.-J. Park, M. Kim, Y.-C. Joo, *NPG Asia Mater.* **2016**, *8*, e250.
- [29] C. Schindler, S. C. P. Thermadam, R. Waser, M. N. Kozicki, *IEEE Trans. Electron Devices* **2007**, *54*, 2762.
- [30] M. N. Kozicki, C. Gopalan, M. Balakrishnan, M. Mitkova, *IEEE Trans. Nanotechnol.* **2006**, *5*, 535.
- [31] P. E. Blöchl, *Phys. Rev. B* **1994**, *50*, 17953.
- [32] G. Kresse, J. Furthmüller, *Phys. Rev. B* **1999**, *54*, 11169.
- [33] S. M. Sze, D. C. Mattis, *Physics of Semiconductor Devices*, John Wiley & Sons, Inc., New York **1981**.
- [34] H. B. Michaelson, *J. Appl. Phys.* **1977**, *48*, 4729.
- [35] L. J. Brillson, Y. Lu, *J. Appl. Phys.* **2011**, *109*, 121301.
- [36] T. Kamiya, K. Nomura, M. Hirano, H. Hosono, *Phys. Status Solidi C* **2008**, *5*, 3098.
- [37] T. Kamiya, K. Nomura, H. Hosono, *Phys. Status Solidi A* **2009**, *206*, 860.
- [38] R. Waser, R. Dittmann, G. Staikov, K. Szot, *Adv. Mater.* **2009**, *21*, 2632.
- [39] W. Guan, M. Liu, S. Long, Q. Liu, W. Wang, *Appl. Phys. Lett.* **2008**, *93*, 223506.
- [40] J. J. Yang, D. B. Strukov, D. R. Stewart, *Nat. Nanotechnol.* **2013**, *8*, 13.
- [41] M.-C. Chen, T.-C. Chang, C.-T. Tsai, S.-Y. Huang, S.-C. Chen, C.-W. Hu, S. M. Sze, M.-J. Tsai, *Appl. Phys. Lett.* **2010**, *96*, 262110.
- [42] M.-S. Kim, Y. H. Hwang, S. Kim, Z. Guo, D.-I. Moon, J.-M. Choi, M.-L. Seol, B.-S. Bae, Y.-K. Choi, *Appl. Phys. Lett.* **2012**, *101*, 243503.
- [43] M.-C. Chen, T.-C. Chang, S.-Y. Huang, G.-C. Chang, S.-C. Chen, H.-C. Huang, C.-W. Hu, S. M. Sze, T.-M. Tsai, D.-S. Gan, F.-S. Yeh, M.-J. Tsai, *Electrochem. Solid-State Lett.* **2011**, *14*, H475.
- [44] N. Xu, L. Liu, X. Sun, X. Liu, D. Han, Y. Wang, R. Han, J. Kang, B. Yu, *Appl. Phys. Lett.* **2008**, *92*, 232112.
- [45] Y. C. Yang, F. Pan, Q. Liu, M. Liu, F. Zeng, *Nano Lett.* **2009**, *9*, 1636.
- [46] Y. Aoki, C. Wiemann, V. Feyer, H.-S. Kim, C. M. Sschneider, H. I. Yoo, M. Martin, *Nat. Commun.* **2014**, *5*, 3473.
- [47] C. Rohde, B. J. Choi, D. S. Jeong, S. Choi, J.-S. Zhao, C. S. Hwang, *Appl. Phys. Lett.* **2005**, *86*, 262907.
- [48] A. Mehonic, A. Vrajitoarea, S. Cuffe, S. Hudziak, H. Howe, C. Labbé, R. Rizk, M. Pepper, A. J. Kenyon, *Sci. Rep.* **2013**, *3*, 2708.
- [49] A. Bid, A. Bora, A. K. Raychaudhuri, *Phys. Rev. B* **2006**, *74*, 035426.
- [50] R. Waser, *Nanoelectronics and Information Technology: Advanced Electronic Materials and Novel Device*, Wiley-VCH, Weinheim, Germany **2012**.
- [51] L. D. Bozano, B. W. Kean, M. Beinhoff, K. R. Carter, P. M. Rice, J. C. Scott, *Adv. Funct. Mater.* **2005**, *15*, 1933.
- [52] G. Dearnaley, D. V. Morgan, A. M. Stoneham, *J. Non-Cryst. Solids* **1970**, *4*, 593.
- [53] P. Kuisma-Kursula, *X-Ray Spectrom.* **2000**, *29*, 111.
- [54] A. B. Chen, S. G. Kim, Y. Wang, W. S. Tung, I. W. Chen, *Nat. Nanotechnol.* **2011**, *6*, 237.
- [55] O. J. Gregory, I. M. Tougas, M. Amani, E. E. Crisman, *ACS Comb. Sci.* **2013**, *15*, 580.
- [56] B. W. David, C. B. Carter, *Transmission Electron Microscopy*, Springer, Boston, MA **2009**.
- [57] D. Son, J. Lee, S. Qiao, R. Ghaffari, J. Kim, J. E. Lee, C. Song, S. J. Kim, D. J. Lee, S. W. Jun, S. Yang, M. Park, J. Shin, K. Do, M. Lee, K. Kang, C. S. Hwang, N. Lu, T. Hyeon, D.-H. Kim, *Nat. Nanotechnol.* **2014**, *9*, 397.
- [58] R. E. Galindo, R. Gago, D. Duday, C. Palacio, *Anal. Bioanal. Chem.* **2010**, *396*, 2725.
- [59] K. Nomura, T. Kamiya, H. Ohta, T. Uruga, M. Hirano, H. Hosono, *Phys. Rev. B* **2007**, *75*, 035212.
- [60] H. Noh, K. J. Chang, B. Ryu, W. Lee, *Phys. Rev. B* **2011**, *84*, 115205.
- [61] P. M. Fahey, P. B. Griffin, J. D. Plummer, *Rev. Mod. Phys.* **1989**, *61*, 289.
- [62] J. E. Medvedeva, C. L. Hettiarachchi, *Phys. Rev. B* **2010**, *81*, 125116.
- [63] T. Kamiya, K. Nomura, H. Hosono, *Phys. Status Solidi A* **2010**, *207*, 1698.
- [64] I. Barin, O. Knacke, O. Kubaschewski, *Thermochemical Properties of Inorganic Substances*, Springer, Berlin, Germany **1973**.
- [65] G. Kresse, D. Joubert, *Phys. Rev. B* **1999**, *59*, 1758.
- [66] J. P. Perdew, K. Burke, M. Ernzerhof, *Phys. Rev. Lett.* **1996**, *77*, 3865.
- [67] Y. Kang, S. H. Jeon, Y.-W. Son, Y.-S. Lee, M. Ryu, S. Lee, S. Han, *Phys. Rev. Lett.* **2012**, *108*, 196404.
- [68] S. Lany, *Phys. Rev. B* **2013**, *87*, 085112.